RSC Advances

ROYAL SOCIETY OF CHEMISTRY

www.rsc.org/advances

[TOC only]

Single wall carbon nanohorn (SWCNH)/Graphene nanoplate/Poly(methyl methacrylate) Nanocomposites: A Promising Material for Electromagnetic Interference Shielding Applications

Ranadip Bera, Sumanta Kumar Karan, Amit Kumar Das, Sarbaranjan Paria and Bhanu Bhusan Khatua*

Materials Science Centre, Indian Institute of Technology, Kharagpur-721302, India

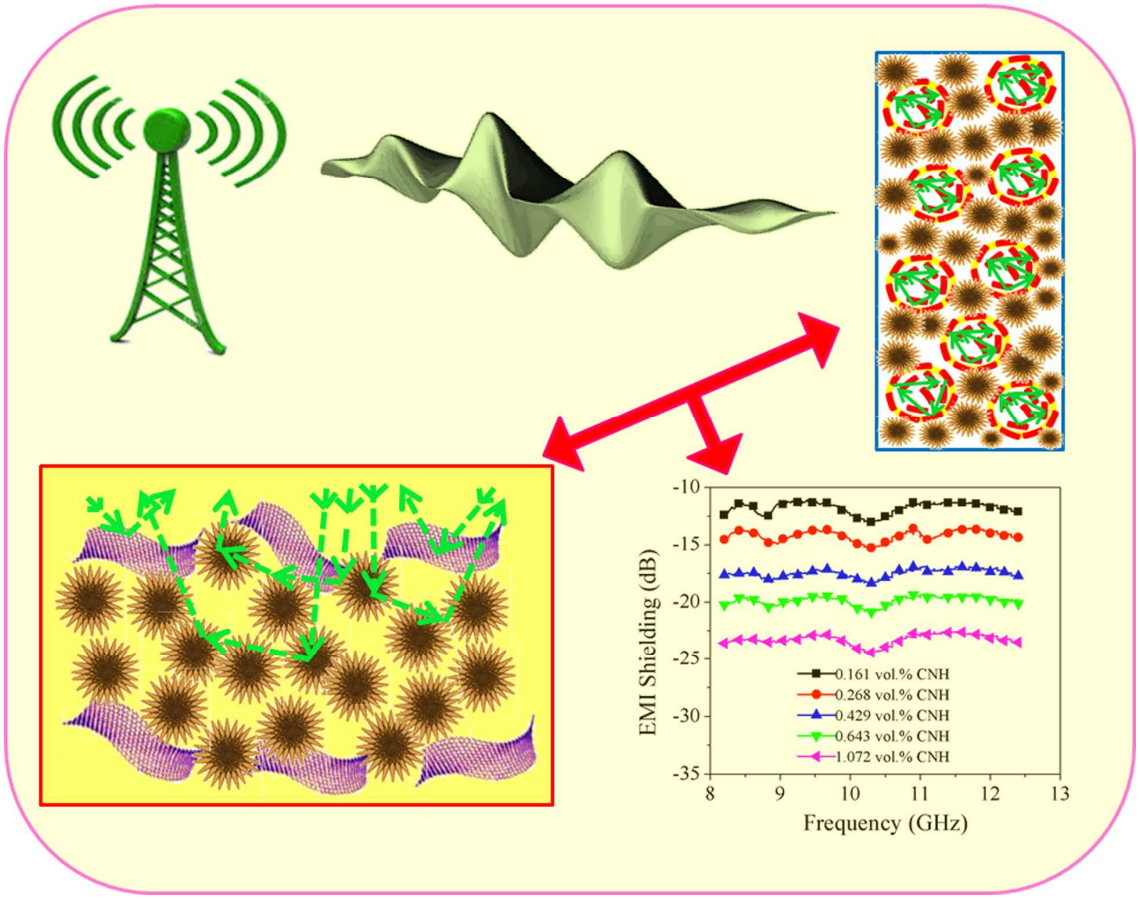

Single wall carbon nanohorn (SWCNH)/Graphene nanoplate/Poly(methyl methacrylate) Nanocomposites: A Promising Material for Electromagnetic Interference Shielding Applications

Ranadip Bera, Sumanta Kumar Karan, Amit Kumar Das, Sarbaranjan Paria and Bhanu Bhusan Khatua*

Materials Science Centre, Indian Institute of Technology, Kharagpur-721302, India

*Corresponding author. Tel.: 91 3222 283982, E-mail address: khatuabb@matsc.iitkgp.ernet.in (B. B. Khatua).

Abstract

Single wall carbon nanohorn (SWCNH)/graphene nanoplates (GNP)/poly(methyl methacrylate) (PMMA) nanocomposites were prepared through *in-situ* bulk polymerization of SWCNH dispersed methyl methacrylate monomer, followed by addition of suspension polymerized nonconductive GNP/PMMA bead during the polymerization. Three dimensional continuous network of GNP-SWCNH-GNP or SWCNH-GNP-SWCNH has been formed throughout the PMMA matrix outside the GNP/PMMA beads that played a crucial role for high electrical conductivity and electromagnetic interference shielding effectiveness (EMI SE) in the nanocomposites. Thus, high electrical conductivity (4.54×10^{-2} S.cm^{-1}) and high EMI SE value ~ (-23.6 dB) were achieved in the nanocomposites even at a low loading of SWCNH and GNP. The ratio of volume (vol %) and weight (wt %) of the all the components (SWCNH:GNP:PMMA) in the final nanocomposites were 1.072:0.089:98.839 and 1.0:0.175:98.825, respectively. The GNP/PMMA beads act as excluded volume and also attenuates the microwave energy through multiple reflections. The nonconductive GNP/PMMA beads also create dielectric mismatch which influences the internal multiple reflection property of the nanocomposites.

Keywords: Single wall carbon nanohorn, EMI shielding, Conductivity, Microwave attenuate.

Introduction

Recently considerable research interest has been put on the electromagnetic interference (EMI) shielding application due to rapidly increasing electromagnetic pollution by enormous number of different electromagnetic wave devices. Different electromagnetic wave devices, such as communication equipment, wireless networks, and modern electronic gadgets emit high intense electromagnetic field which interacts with other devices and creates serious EMI problems. Restriction of both incoming and outgoing electrical and magnetic fields by lightweight materials is the main need of a good shielding material, especially in the area of aircraft, aerospace, automobiles, and fast-growing next-generation electronics. For this type of material application, conductive nanofiller based polymer nanocomposites are more suitable (light weight, low cost, excellent proccessibility and broad absorption bandwidth properties) rather than conventional metal based EMI shielding materials.

Previously, carbon based conductive nanofillers like CNT,[1] graphene, carbon black etc. were incorporated (through *in-situ* polymerization of monomers, melt mixing and solution blending process) into the matrix polymer to prepare efficient EMI shielding materials. Liu et al. prepared CNT/polyurethane nanocomposites and achieved ~17 dB EMI SE value at ~20 wt% of SWCNT loading.[2] Reduced graphene oxide (rGO) based, rGO/polystyrene (PS) nanocomposites revealed EMI SE value of ~45.1dB at 3.47 vol% loading of rGO.[3] Joo et al.[4] reported an EMI SE value of ~27 dB at 40 wt% loading of MWCNT in solution blended MWCNT/poly (methyl methacrylate) (PMMA) nanocomposites. The nanocomposites with maleic anhydride modified MWCNTs and PMMA, prepared by the *in-situ* and *ex-situ* solution polymerization, showed EMI SE value of 11 dB at 2.44 wt% MWCNT loading[5]. An EMI SE value of ~20 dB has been reported in solution blended MWCNT/PS nanocomposites at 7 wt% MWCNT loading.[6] Epoxy

resin/SWCNT nanocomposites shows 20~30 dB EMI SE value at ~15wt% loading of SWCNT in the X-band region.[7] An EMI SE value of ~19 dB was obtained by Gupta et al.[8] at 15 wt% of carbon nano-fiber (CNF) loading in CNF/PS nanocomposites. Porous graphene/PS nanocomposites containing functionalize graphene sheet showed EMI SE value of ~29 dB at 30 wt% CNF loading.[9]

The extent of reflection, absorption and internal multiple reflection of radiation together represents the total EMI SE of a material. The presence of conductive nanofiller in the nanocomposites creates a significant impedance mismatch between air and materials which is the cause of microwave reflection by the materials. The conductive nanofillers facilitates in dissipation or absorption of electromagnetic radiation in the materials through conductive network path. The microwave energy attenuates through multiple reflections which happen due to the in-homogeneity within the materials[10]. So, through the scattering of microwave and increasing the conductive network in the nanocomposites one can enhance the reflection and absorption of microwave. To fulfill the said criteria of a good EMI shielding material, flower like structure single wall carbon nanohorn (SWCNH) and graphene nanoplate (GNP, plate like structure) have been chosen as fillers in our current study. GNP possesses excellent electrical, mechanical, thermal conductor and barrier properties due to their unique size and morphology. SWCNH consisting of a dahlia flower like architecture (due to self-assembling.[11]) with an average diameter of about 80 nm[12] and has high electrical conductivity, very high surface area. Individual nanohorn looks like a horn with a variable diameter of 2~5 nm, length of 40~50 nm[13] and horn tip has an average angle of ~ 20^{o}.[14] The electrical property of SWCNH comes out from its structural arrangement. Berber et al.[15] and Kolesnikov et al.[16] explained the electrical property of SWCNH. However, the main disadvantage of this filler is high cost and low dispersibility in

high viscous polymer melt. To overcome this disadvantage, here, we demonstrate a conventional easy technique to prepare hybrid nanocomposites.

On the other hand, the properties of PMMA (high dimensional stability, good optical clarity, and high weather ability property) and easy synthesis process in lab influence us to choose it as matrix material in our work. Here, the aim of our work is to obtain high EMI SE and electrical properties of SWCNH/GNP/PMMA nanocomposites, prepared through *in-situ* bulk polymerization of SWCNH dispersed methyl methacrylate in the presence of suspension polymerized GNP/PMMA beads at low loading of nanofillers. In the final nanocomposites two separate phases have been created; SWCNH containing continuous PMMA phase and GNP containing PMMA beads. As both the phases in the nanocomposites consisting of same matrix polymer (PMMA), there is no phase separation but both acting differently. The EMI SE and conductivity enhanced due to the presence of GNP/PMMA beads which act as exclude volume in the nanocomposites. The microwave energy attenuates through absorption (using SWCNH-GNP-SWCNH conductive network) and multiple internal reflection due to the presence of GNP/PMMA beads. Thus, very high EMI shielding value ~ (-23.6 dB) was achieved at an extremely low loading of SWCNH and GNP in the nanocomposites. The ratio of SWCNH:GNP:PMMA in the final nanocomposites was 1.072 vol% (1.0 wt%) : 0.089 vol% (0.175 wt%) : 98.839 vol% (98.825 wt%).

Experimental section

Materials Details

Methyl methacrylate (MMA) monomer (synthetic grade, M = 100.12g/mol, d = 0.94 kg/l, purity> 99%) was obtained from Merk, Germany. Benzoyl peroxide (BP) and polyvinyl alcohol (PVA) were procured from Merck, India. SWCNH (purity >99%, horn diameter 3~5 nm, cluster

diameter 60~120 nm, active surface 250~300 m^2/gm) and graphite nanoplate (GNP) (multilayer, carbon purity >99.5%, diameter 5~25 μm, thickness 8~10 nm) were purchased from J. K. Impex, Mumbai, India. The GNP and SWCNH were used as received without any chemical modification.

Preparation of SWCNH/GNP/PMMA Nanocomposites

Purified MMA monomer (purification process in SI) was used to prepare the nanocomposites. The GNP containing PMMA bead was prepared through suspension polymerization method. To optimize the polymerization process and final weight of the product, the suspension polymerization MMA monomer without GNP loading was done for three times. Following the optimized process, the GNP loaded PMMA bead was prepared. Initially GNP (calculated amount 0.1g, 0.212 wt% with respect to monomer) dispersed in purified MMA monomer (50 ml, 47g) by ultrasoinication for 2 h at room temperature. Subsequently, the polymerization initiator BP was dissolved in GNP dispersed MMA monomer in stirring condition. Nitrogen (N_2) inlet and refluxing condenser fitted with a three neck glass reactor containing 900 ml PVA-water (suspension stabilizer) solution was placed in an oil bath, positioned on a temperature controlled magnetic stirrer. The GNP/MMA/BP mixture was added into the reactor in N_2 atmosphere under constant stirring. The reactor temperature was gradually increased up to 70 ^oC and the reaction was continued for 2 h. After completion of the reaction, the mixture was cooled and the beads are sieved. The desire sieved beads (GNP containing PMMA beads) were washed by methanol, followed by drying through keeping it in a hot air oven at 50 ^oC for 36 h. The GNP loading (0.128 vol%, 0.25 wt%) was calculated form the weight of GNP/ PMMA bead (40 g). In this work, a fixed GNP content (< Pc value) was maintained to eliminate its role in preparing conducting path through in the bead rather to create significant

mismatch in the dielectric property of the nanocomposites which facilitates high EMI shielding efficiency of the nanocomposites.

Finally, a SWCNH/GNP/PMMA nanocomposite was prepared using suspension polymerized GNP/PMMA bead through *in-situ* bulk polymerization process. The bulk polymerization reaction was carried out in an isolated system. Initially, SWCNH (0.036 g, 0.255 wt% with respect to monomer) was dispersed in the purified MMA monomer (15 ml, 14.1g) using probe ultrasonicator for 2 h at room temperature. Subsequently the SWCNH dispersed MMA monomer was poured into N_2 inlet and a refluxing condenser fitted a three neck reactor, placed in an oil bath positioned on a temperature controlled magnetic stirrer. BP was added into the reactor under constant stirring condition and the temperature was increased to ~70 ^{o}C under N_2 atmosphere. The reaction mixture started to form viscous (i.e. the monomer started to form the oligomer) after 30 min of the polymerization reaction. The GNP/PMMA bead (12 g) was gradually added in the reaction mixture at the viscous condition. The reaction was allowed for 1 h at the same reaction condition to obtain the final nanocomposites. The resulting nanocomposites was air dried for 24 h at room temperature followed by drying in a hot air oven at 50 ^{o}C for 36 h. The content of SWCNH (~0.161 vol%, ~0.15 wt%) and GNP/PMMA bead (50 vol%, ~50 wt%) were calculated from the final weight (24 g) of the SWCNH/GNP/PMMA nanocomposites.

SWCNH/GNP/PMMA nanocomposites with various amounts, such as, ~0.161 vol% (~0.15 wt%), 0.268 vol% (~0.25 wt%), 0.429 vol% (~0.4 wt%), 0.643 vol% (~0.6 wt%) and 1.072 vol% (~1.0 wt%) of SWCNH at constant GNP/PMMA bead loading and various amounts [50 vol% (~50 wt%), 60 vol% (~60 wt%), and 70 vol% (~70 wt%)] of GNP/PMMA bead at constant SWCNH loading were prepared with the same method. Finally, all the nanocomposites

were compression molded in a hot press under constant pressure (2 MPa) at 200 ^{o}C, followed by natural cooling to room temperature. Figure 1 schematically represents the method of preparation of the SWCNH/GNP/PMMA nanocomposites.

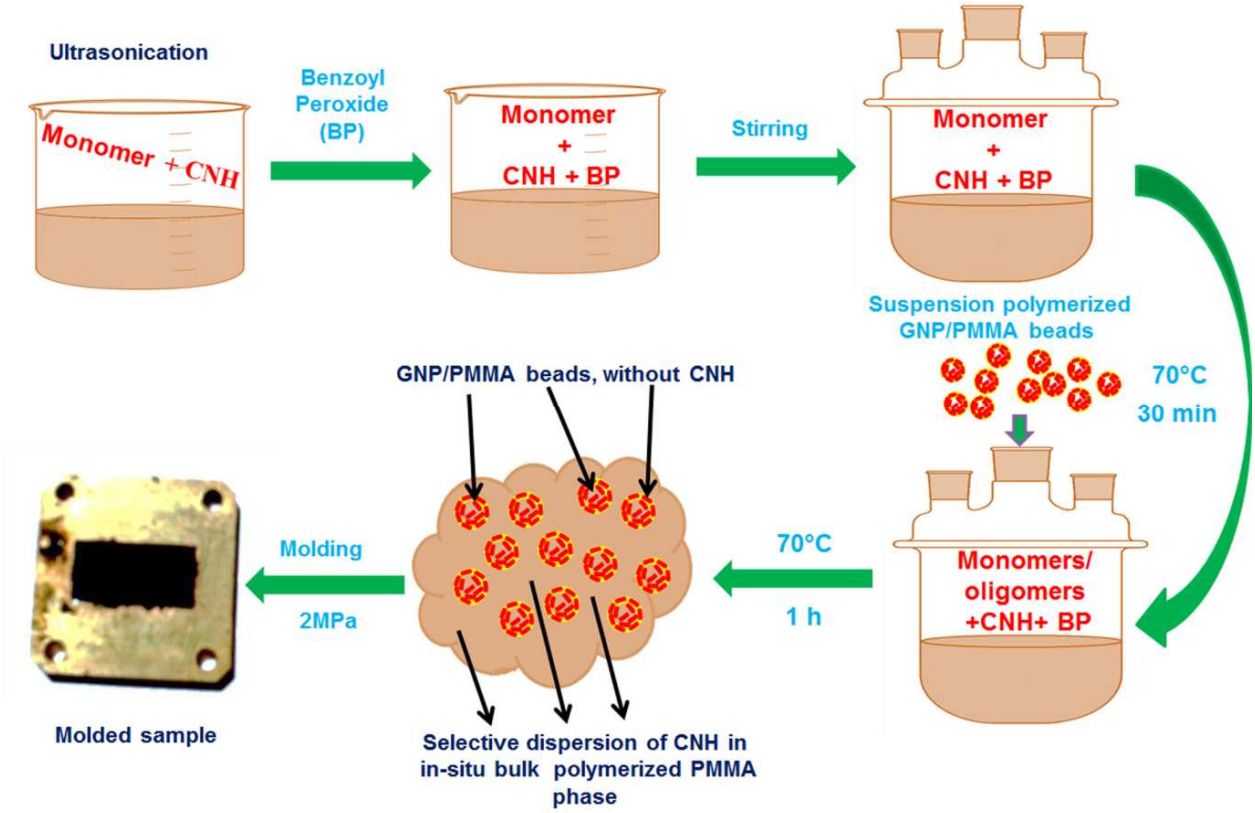

Figure 1: Schematic for the preparation of SWCNH/GNP/PMMA nanocomposites

Characterization

The morphological analysis of the SWCNH/GNP/PMMA nanocomposites was investigated by field emission scanning electron microscope (FESEM: Carl Zeiss-SUPRA 40, operated at an accelerating voltage of 5kV) and high resolution transmission electron microscope (HRTEM, JEM-2100, JEOL, Japan) operated at an accelerating voltage of 200 kV. A scanning electron microscope (SEM, VEGAII LSU, TESCAN, Czech Republic) was used to study the size of GNP/PMMA bead. The thermal stability of the synthesized pure PMMA and its nanocomposites with GNP and SWCNH was studied in air atmosphere in the temperature range

of 30 – 600 °C, with a heating rate of 10 °C/min, employing a TGA V 50 IA Dupont 2100 thermo gravimetric analyzer (discussed in SI). The tensile properties of the synthesized pure PMMA and its nanocomposites with GNP and SWCNH were measured by a Tinius Olsen H 50 KS universal testing machine. Tensile study was carried out on dumb-bell shaped injection molded samples at room temperature with a gauge length of 36 mm, width 5.9 mm, thickness 2.5 mm and crosshead speed of 5 mm/min. The reported values are the average value of four specimens (discussed in SI).

The electrical conductive character (DC conductivity, σ_{DC}) of the SWCNH/GNP/PMMA nanocomposites was done by following the two probe technique on the compress molded bar (10~30 × 10 × 3 mm^3) sample. The σ_{DC} value of the nanocomposites was calculated by the following equation (1).

$$\sigma_{DC} = IL/VA \qquad (1)$$

Current, voltage and length of the samples are symbolized respectively as I, V and L in the above equation.

EMI shielding effectiveness (SE) of the compression molded SWCNH/GNP/PMMA nanocomposites slabs (25.5 × 13 × 2~4 mm^3) was measured by an E5071C ENA series network analyzer (Agilent Technologies). To perform this study, the rectangular specimens were placed between the two ports of the waveguide. The total SE, shielding by absorption and shielding by reflection of the nanocomposites were calculated from the recorded S parameter (S_{11}, S_{12}, S_{21}, S_{22}) in the X band (8.2–12.4 GHz) frequency range.

The total EMI SE (SE_T) refers to the logarithm of the ratio of incident power (P_{in}) and transmitted power (P_{out}).

$$SE_T(dB) = 10\,log\,P_{in}/P_{out} \qquad (2)$$

The incident power of the radiation gets divided into three parts (absorbed power: P_{abs}, reflected power: P_{ref}, P_{out}) after striking the material.

$$P_{abs} = P_{in} - P_{ref} - P_{out} \quad (3)$$

$R = P_{ref} / P_{in}$, $A = P_{abs} / P_{in}$ and $T = P_{out} / P_{in}$ are the power coefficients. These are related through the following relation:

$$A + T + R = 1 \quad (4)$$

The total EMI SE (SE_T) value is obtained from shielding efficiency by absorption, reflection and multiple internal reflections of radiation (SE_A, SE_R, and SE_M), as expressed in the following equation:

$$SE_T = SE_A + SE_R + SE_M \quad (5)$$

The above equation (equation 5) becomes the following equation (6) when $SE_T \geq 15$ dB (SE_M becomes negligible).[17]

$$SE_T \approx SE_A + SE_R \quad (6)$$

The vector network analyzer, connected with wave guide tubes, attached with quadrilateral sample holder, simultaneously measures the reflected and transmitted power at the two parts over the 8.2–12.4 GHz frequency range. The scattering parameters S were measured by the device. These scattering parameters are the measurement of power coefficient: R = $|S_{11}|^2$ i.e. P_{in} normalized by the power reflected back at port 1, T = $|S_{21}|^2$ is related to the normalize power transmitted from port 1 to port 2 through the device.[18] If the material is homogeneous in nature S_{11} should be equal to S_{22}, and S_{21} also should be equivalent to S_{12}. Thus the ratio of the power absorbed by the sample (P_{abs}) to source power can be expressed by the following expression as,

$$T = |S_{21}|^2 = |S_{12}|^2 \quad (7)$$

$$R = |S_{11}|^2 = R = |S_{22}|^2 \quad (8)$$

In terms of the power of the effective incident electromagnetic wave inside the shielding material, the reflectance and effective absorbance can be conveniently expressed as: [19]

$$SE_R = -10logR \quad (9)$$

$$SE_R = -10\,log(1-R) = 10log(1/1-|S_{11}|^2) \quad (10)$$

$$SE_A = 10log|1-|S_{11}|^2/|S_{12}|^2| \quad (11)$$

The total EMI SE was calculated using the following equation:

$$SE_{total} = -10logT = -10log|S_{21}|^2 \quad (12)$$

Following a MATLAB code based on Nicolson-Ross-Weir method[20], the complex permittivity and permeability were evaluated from S parameter of the sample slab. The Ac conductivity of the composite calculated from complex permittivity and discussed in SI.

Results and Discussion

Morphology

The FESEM image of the SWCNH/GNP/PMMA nanocomposites is shown in Figure 2 (a). The FESEM image displays the existence of SWCNH and GNP plates which help to form SWCNH-GNP-SWCNH conducting network in the nanocomposites. SWCNH was selectively dispersed in the *in-situ* bulk polymerized PMMA phase and the rare penetration of SWCNH inside the GNP/PMMA beads is evident from this image. The *in-situ* bulk polymerized PMMA region clearly displays the existence of SWCNH in its higher magnification image (Figure 2c). This high magnification image revealed that SWCNHs were dispersed homogeneously throughout the host polymer. The higher magnification image (figure 2d) of the GNP/PMMA bead region clearly reveals the existence of GNP in the bead region. The TEM image (Figure 2 b, e, and f) of SWCNH/GNP/PMMA nanocomposites also supports the presence of SWCNH in

the continuous PMMA phase of the nanocomposites. The formation of SWCNH-GNP-SWCNH conductive network throughout the SWCNH/GNP/PMMA nanocomposites can be clearly seen

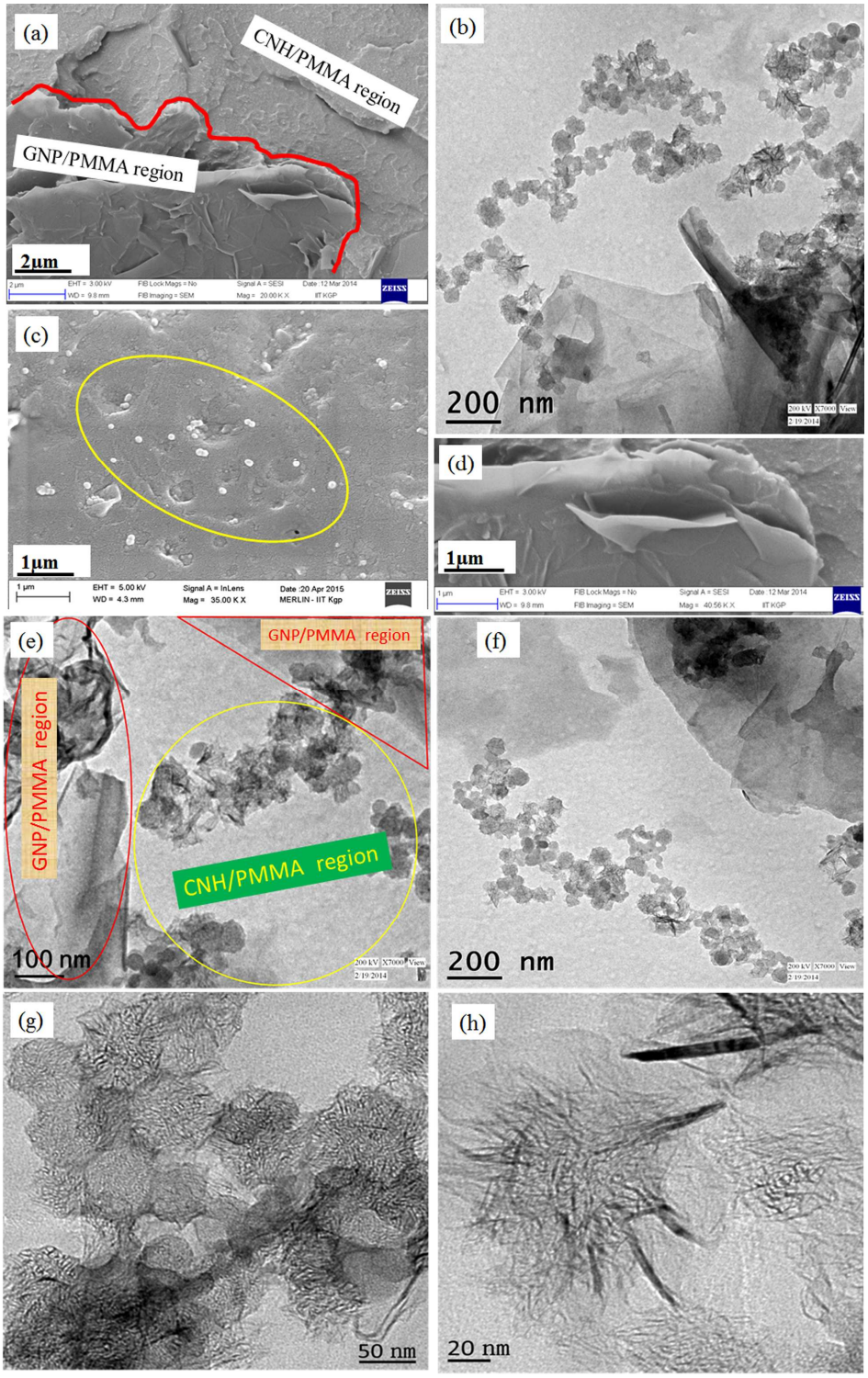

Figure 2: FESEM image of (a) GNP/PMMA bead and SWCNH/PMMA junction, (c) SWCNH/PMMA bulk polymerized region, (d) GNP/PMMA bead region and (b, e, f) TEM image of the SWCNH/GNP/PMMA nanocomposites. (g) and (h) TEM image of SWCNH.

in the TEM image. Due to van der Walls force of interaction, SWCNH tends to agglomerate and has got flower like structure. In this work, SWCNH was highly dispersed in the monomer due to long time sonication before polymerization. The secondary agglomeration phenomena of SWCNH occur during the polymerization process when the viscosity increases in the reactor.[21] Due to secondary agglomeration, the multiple contact points of flower like SWCNH formed SWCNH-SWCNH network throughout the nanocomposites. The contact between individual SWCNH to form the SWCNH network throughout the bulk polymerized PMMA phase is presented in Figure S1(b) of SI. The highly symmetrical single wall flower like architecture can be well depicted from the TEM image (Figure 2g and 2h).

The SEM image of suspension polymerized GNP/PMMA bead is presented in Figure S1(a) of SI. The average diameter of the GNP/PMMA bead is 500 μm, as measured by Vega TC software.

Electrical analysis (DC Conductivity Measurement)

Figure 3 displays the variation of (σ_{DC}) of the SWCNH/GNP/PMMA nanocomposites with SWCNH and GNP/PMMA bead loadings. As can be seen, the σ_{DC} value of SWCNH/GNP/PMMA nanocomposites increases with the increase of SWCNH loading (shown in figure 3a) as well as *in-situ* suspension polymerized GNP/PMMA bead loading (shown in figure 3b). In this work, we optimized the bead loading (70 vol%) in the nanocomposites where the highest σ_{DC} value was achieved at constant SWCNH loading. Thus we reached an optimum σ_{DC} value (4.54×10^{-2} S.cm^{-1}) through 1.072 vol% SWCNH and 70 vol% GNP/PMMA bead

loadings in the SWCNH/GNP/PMMA nanocomposites. Throughout this optimization step, we observed, below 50 vol% GNP/PMMA bead loading, the SWCNH/GNP/PMMA nanocomposites behaves like an insulating polymer, and shows ~1.1×10^{-11} S.cm^{-1} electrical conductivity at 0.161 vol% SWCNH loading. A remarkable improvement in the electrical conductivity (~7.4×10^{-6} S.cm^{-1}) was evident at the same SWCNH loading (0.161 vol%) after the addition of 50 vol% GNP/PMMA bead loading in the nanocomposites. However, maximum σ_{DC} value of the nanocomposites was achieved in the presence of 70 vol% GNP/PMMA bead loading. Beyond 70 vol% GNP/PMMA bead loading, the conductivity of the nanocomposites started decreasing at a particular SWCNH loading.

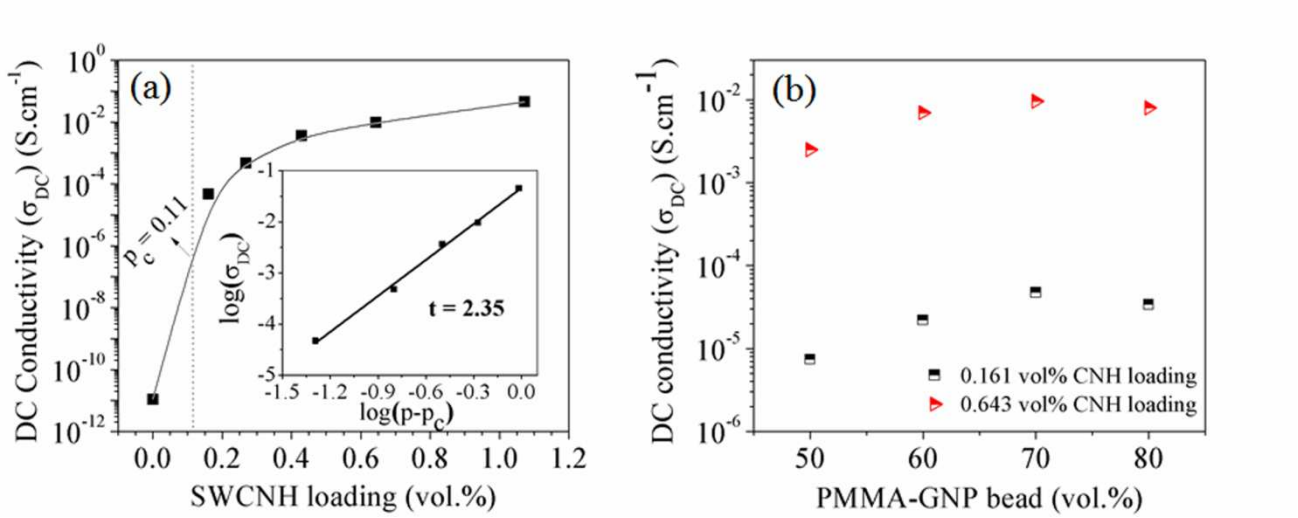

Figure 3: (a) DC conductivity of the SWCNH/GNP/PMMA nanocomposites with various SWCNH loadings at 70 vol% percent of bead loading. The straight line in the inset of figure 3a is the log–log plot of σ_{DC} *versus* (p–p_c), fitted by the least–squares method using equation (13). It gives the best fit values p_c = ~0.11vol%. (b) The variation of DC conductivity with various GNP/PMMA bead loading in the SWCNH/GNP/PMMA nanocomposites.

It is assumed that, the prepared nanocomposites become conductive and achieved such a high electrical conductivity after the addition of the GNP/PMMA beads in the bulk polymerized SWCNH/PMMA phase due to two important phenomena. Firstly, the presence of GNP/PMMA bead in the SWCNH/PMMA bulk polymerized region concise the SWCNH/PMMA region and thus the effective concentration of the SWCNH significantly increases in the SWCNH/PMMA bulk polymerized region. This phenomenon facilitates in the formation of SWCNH-SWCNH conductive path all over the nanocomposites. Moreover, it is assumed that due to the presence of GNP/PMMA bead, an interconnected conductive network SWCNH-GNP-SWCNH or GNP-SWCNH-GNP also formed at the outer surface of GNP/PMMA bead in the nanocomposites. The swelling of GNP/PMMA bead during polymerization facilitates the rarely penetration of SWCNH in the surface of the beads. Thus the GNP (present at the outer surface of the bead) and SWCNH formed the SWCNH-GNP-SWCNH or GNP-SWCNH-GNP conductive network. These two phenomena helps to develop electrical conductivity at 0.161 vol% SWCNH loading in presence of 50 vol% GNP/PMMA bead in the nanocomposites and σ_{DC} values of 4.74×10^{-5} S.cm^{-1} was achieved at 70 vol% GNP/PMMA bead loading even with 0.161 vol% SWCNH loading. To support this assumption, the σ_{DC} values of 0.161 vol% SWCNH and 70 vol% GNP/PMMA bead loaded SWCNH/GNP/PMMA nanocomposites was compared with the PMMA/SWCNH nanocomposites without any GNP/PMMA bead having 0.531 vol% of SWCNH loading, as addition of 70 vol% bead leads to 3.3 times increment in the effective concentration of SWCNH in the nanocomposites. However, the SWCNH/GNP/PMMA nanocomposites with 70 vol% GNP/PMMA bead loading gives much superior σ_{DC} value compared to that without any GNP/PMMA bead. This result supports the formation of more SWCNH-SWCNH conductive path through increase of effective concentration of SWCNH and the SWCNH-GNP-SWCNH or

GNP-SWCNH-GNP interconnected conductive network phenomena. The σ_{DC} value of the nanocomposites gradually decreases above the optimum bead loading (70 vol%) because above this loading the continuity of the SWCNH-SWCNH conductive path gets started to restricted by beads coagulation. As the GNP/PMMA beads are nonconductive, the continuous conductive path in the nanocomposites faces difficulty to contain its continuity through bead coagulation beyond the optimum bead loading.

With the help of percolation theory, the variation of the σ_{DC} value with nanofiller loading in the nanocomposites was explained by several research groups. [22,23] The relation of the σ_{DC} with the percolation threshold (p_c) and the vol% of conducting filler (p) were explained by the power-law equation (13).

$$\sigma_{DC}(p) = \sigma_0(p - p_c)^t \qquad \text{For} \quad p \gg p_c \qquad (13)$$

The inset of Figure 3a, best fitted linear plot of log(σ_{DC}) versus log (p-p_c) was used to calculate the value of critical exponent (t) and 'p_c' for the SWCNH/GNP/PMMA nanocomposites. Thus the p_c~0.11vol% and 't'~2.35 values were obtained for the SWCNH/GNP/PMMA nanocomposites. The p_c value indicates the homogeneous dispersion of nanofillers (SWCNH and GNP) in the nanocomposites and the formation of conductive network at very low loading (~0.11 vol%) of SWCNH. This 't' value ~2.35 for the SWCNH/GNP/PMMA nanocomposites is the proof of SWCNH-GNP-SWCNH/GNP-SWCNH-GNP network structure in the PMMA matrix.[24] It was reported[25,26] that the 't' value also used to predict the nature (2D or 3D) of network. It is predicted that t' value for 2D lattice 'lie between 1.10 and 1.43, and higher than 2.02 for a 3D lattice. Thus 't' value ~2.35 confirms that 3D percolating network path was formed in our prepared SWCNH/GNP/PMMA nanocomposites.

Beyond 0.429 vol% SWCNH loading, the conductivity of the nanocomposites almost remains constant (Figure 3a). Many researchers reported[27] such a similar trend of unaltered electrical conductivity beyond a certain loading of conducting filler in conductive polymer nanocomposites system. This phenomenon happens due to high difference in conductivity between filler and matrix. The conductivity goes to saturate after an optimum loading of filler for these nanocomposites systems. For these nanocomposites, the current carrying capacity increases beyond this optimum loading of filler but the conductivity of the nanocomposites does not increase because the charge carried occur not only through the physical contact between the nanofillers but also through tunneling and hopping in the insulating gaps between the conductive nanofillers in the nanocomposites. Thin polymer layer between nanofillers creates the insulating gap. The tunneling and hooping of electrons occurs from one filler to another through this insulating gap. A resistance induced due to this in nanocomposites and limits the conductivity. The existences of tunneling mechanism in our prepared nanocomposites are discussed in electrical analysis section (Fig. S2) of SI.

Electromagnetic Interference Shielding Effectiveness (EMI SE)

The total EMI shielding performances depends on three mechanisms, viz., reflection, absorption and internal multiple reflection of radiation. Impedance mismatch between air and materials is the cause of reflection of radiation. The free electron or mobile charge carrier (holes) of materials interacts with the incident radiation. The absorption of radiation or the dissipation of energy throughout the materials depends on the dielectric permittivity, thickness, permeability etc. of the materials. The in-homogeneity within the materials is the cause of multiple reflections of radiation. For single phase materials, this is typically ignored. [28] The increased number of layer in the materials causes more internal reflection which enhanced the EMI shielding

performance. The frequency dependent EMI SE of SWCNH/GNP/PMMA nanocomposites increases with increasing SWCNH content (Figure 4a), as well as, with increasing GNP/PMMA bead content (Figure 4b) in the frequency region of 8.2~12.4 GHz (so called X band region). The maximum EMI SE value ~ (-23.6 dB) is achieved for the 1.072 vol% SWCNH and 70 vol% GNP/PMMA bead loaded SWCNH/GNP/PMMA nanocomposites. Our prepared SWCNH/GNP/PMMA nanocomposites (1.072 vol% SWCNH and 70 vol% GNP/PMMA bead) can be used as an efficient EMI shielding material in various commercial and practical purposes because a minimum EMI SE of ~20 dB is required for the materials to be applicable in the commercial grounds. The comparison of EMI SE value of this work with other reported work is described in SI (Table S1).

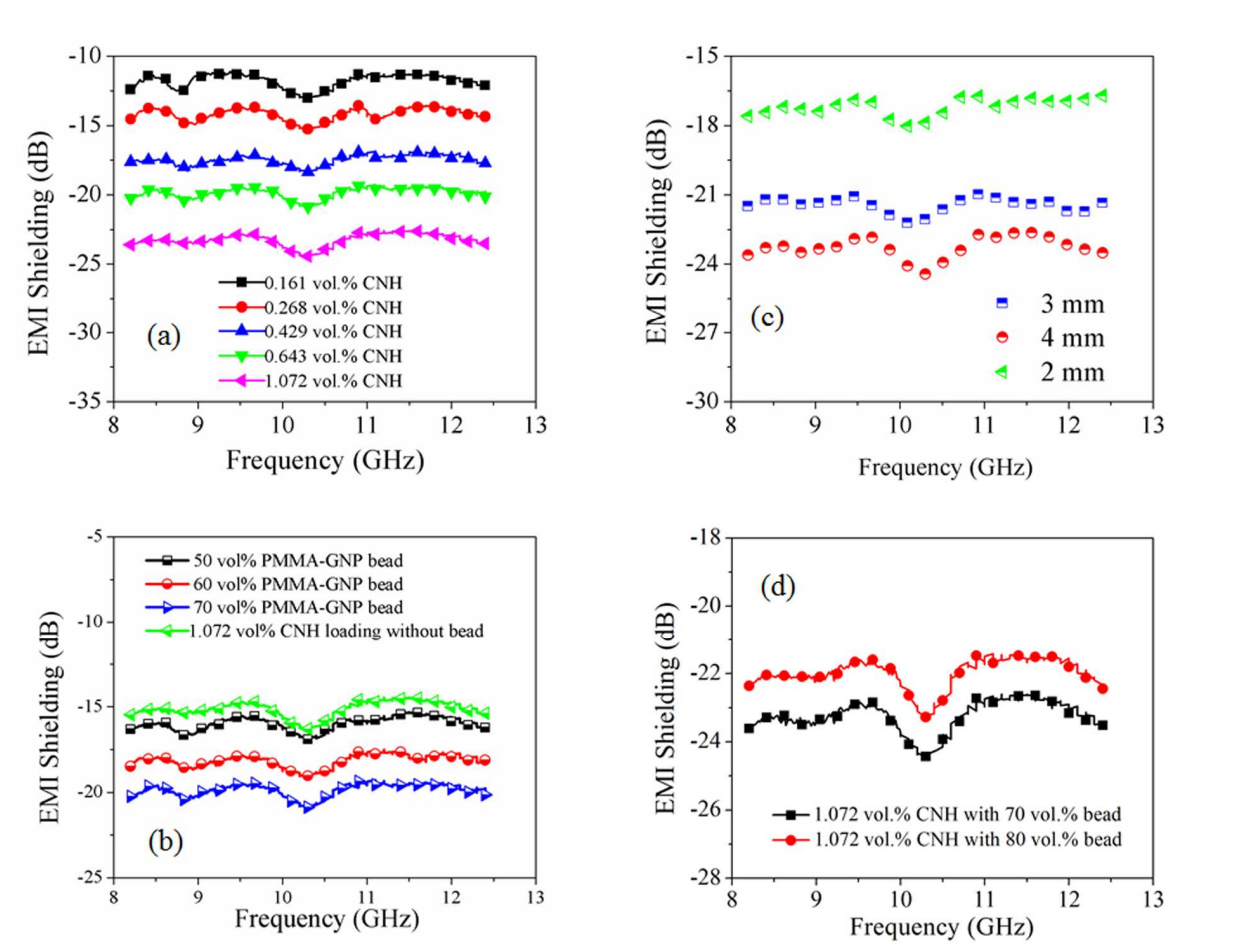

Figure 4: Frequency dependent EMI SE of the SWCNH/GNP/PMMA nanocomposites (4 mm thickness) with (a) various SWCNH loadings at constant (70 vol%) bead loading and (b and d) various GNP/PMMA bead loadings at constant (0.643 vol% and 1.072 vol%) SWCNH loading. (c) The variation of EMI SE with thickness for 1.072 vol% SWCNH and 70 vol% GNP/PMMA bead loaded SWCNH/GNP/PMMA nanocomposites.

Such a high EMI SE value ~(-23.6 dB) of the nanocomposites at considerably low loading of SWCNH can be described in terms of the presence of the GNP/PMMA bead in the bulk polymerized SWCNH/PMMA matrix. The effective concentration of the SWCNH increases in the bulk polymerized SWCNH-PMMA matrix due to concise of matrix phase through the incorporation of GNP/PMMA beads that act as an 'excluded volume'. Thus, the concise matrix phase facilitates the formation of SWCNH-SWCNH conductive path throughout the nanocomposites. Moreover the GNP (presence at the outer surface of the bead) forms SWCNH-GNP-SWCNH or GNP-SWCNH-GNP interconnected conductive network with the concentrated SWCNH around the bead wall, as shown in figure 5. SWCNH rarely penetrate into the outer surface of the GNP/PMMA bead by etching at oligomeric state, but the inside of the bead remains electrically nonconductive i.e. SWCNH fails to enter inside the bead. The SWCNH-SWCNH conductive path and SWCNH-GNP-SWCNH or GNP-SWCNH-GNP interconnected conductive network helps to achieve the EMI SE value through absorption and reflection of electromagnetic wave (figure 6). The microwave absorption property of the nanocomposites is related to the conductivity of the nanocomposites.[19] The conductivity of the nanocomposites increases with the increase of filler loading (as shown in DC conductivity) through the formation of more conductive network and SWCNH–SWCNH conductive path in the nanocomposites. The extent of conductive network formation also increases with the increase of bead loading through

the concise of matrix and the presence of GNP. The conducting nanofillers (SWCNH and GNP) interact with the incident electromagnetic wave and facilitate the electron transport (microwave absorption) throughout the nanocomposites by the conductive network and SWCNH–SWCNH conductive path. Thus EMI SE increases with the increase of SWCNH and GNP/PMMA bead loading in the nanocomposites, as shown in figure 4(a) and 4(b).

Moreover, the presence of nonconductive GNP containing bead in the nanocomposites increases EMI SE through attenuating the incident electromagnetic microwaves by reflecting and scattering between the bead wall and nanofillers, and thus, is difficult for the microwave to escape from the sample before being absorbed, as shown in figure 5. The increase of GNP/PMMA bead loading in the nanocomposites enhance the microwave absorption through internal multiple reflection. The EMI SE values of 1.072 vol% SWCNH containing SWCNH/PMMA nanocomposites without any bead presents the importance of GNP/PMMA bead in the nanocomposites (figure 4b).

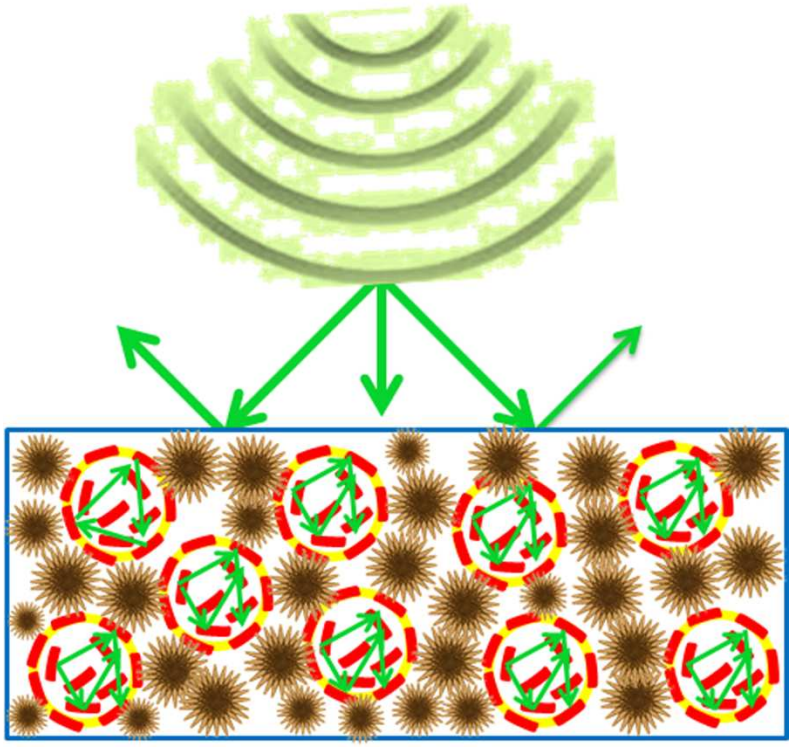

Figure 5: Schematic representation for the effect of GNP/PMMA bead about attenuating the incident electromagnetic microwaves by reflecting and scattering between the bead wall and nanofillers and the concentration of SWCNH at the bead wall in the SWCNH/GNP/PMMA nanocomposites.

The shielding effectiveness depends on the thickness of the materials. The microwave absorption property increases with the increase of materials' thickness. Figure 4c shows that the EMI SE value of the 1.072 vol% SWCNH and 70 vol% GNP/PMMA bead loaded SWCNH/GNP/PMMA nanocomposites increases with its thickness and maximized at a thickness of 4 mm. Figure 6 represents the microwave reflection phenomena in the presence of conductive network structures.

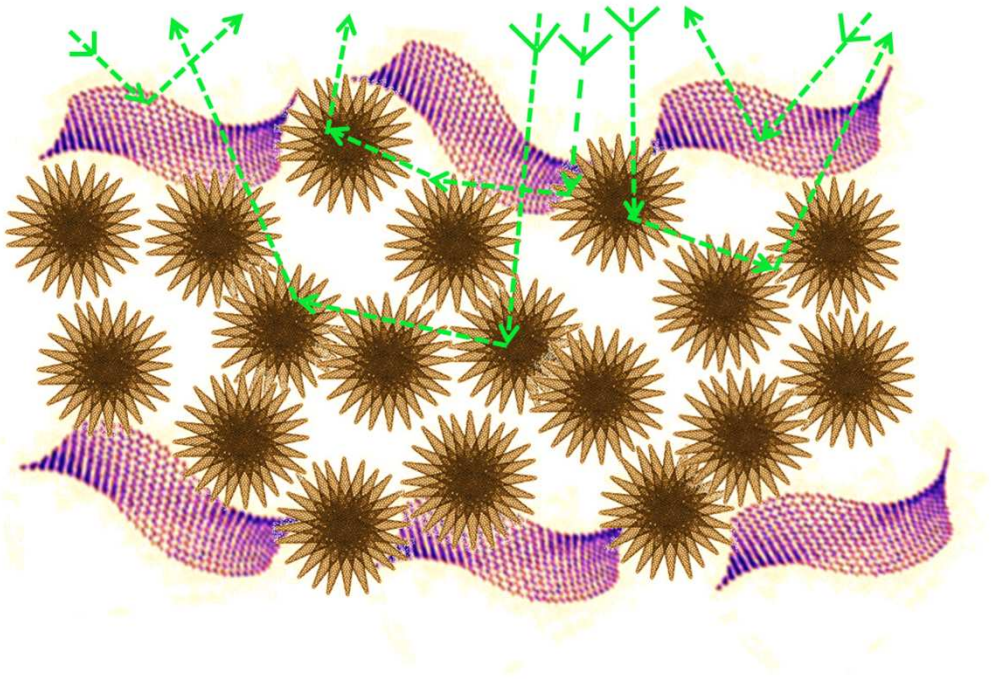

Figure 6: Schematic representation of microwave reflection by SWCNH-GNP-SWCNH network.

Figure 4d displays that the EMI shielding efficiency of the nanocomposite decreased beyond 70 vol% GNP/PMMA bead loading. The GNP/PMMA beads starts collapsing with each other and blocking the continuous conductive network in the nanocomposite with the increase of its' loading beyond 70 vol%. As we know the GNP loading in the bead is below percolation point, due to the blocking of continuous conductive network in the matrix the conductivity of the nanocomposite decreases (shown in figure 3b), and hence, lowers the EMI SE value. On the other hand due to bead collapsing the absorption of microwave through multiple reflections is also affected.

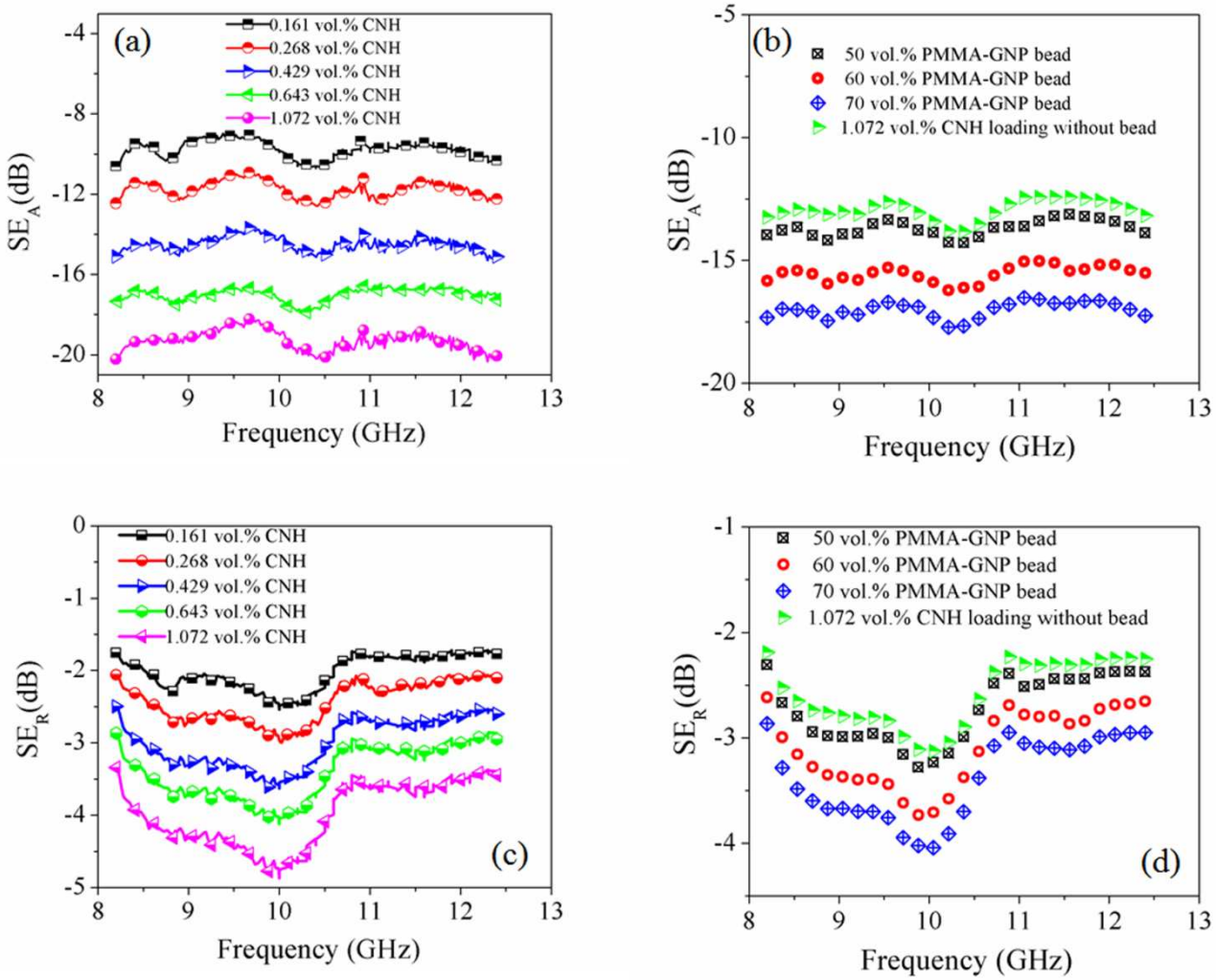

Figure 7: Variation of SE_A with (a) various SWCNH content at constant GNP/PMMA bead loading (70 vol%) and (b) various GNP/PMMA bead loading at constant SWCNH loading (0.643 vol%). Variation of SE_R with (c) different loading of SWCNH at constant GNP/PMMA bead loading (70 vol%) and (d) different loading of GNP/PMMA bead at constant SWCNH loading(0.643 vol%). All measurement of the SWCNH/GNP/PMMA nanocomposites done in X band frequency region with 4 mm thickness.

The contribution of and SE_R and SE_A in the total EMI SE value is illustrated in Figure 7. The contribution of SE_A in the EMI SE is higher than SE_R. The similar result ($SE_A > SE_R$) for different types of polymer nanocomposites has also been reported by many researchers.[29,30,31] The ability of microwave absorption or dissipation of energy increases in the nanocomposites with the increasing amount of SWCNH through the formation of more SWCNH-SWCNH conductive paths and the SWCNH-GNP-SWCNH conductive network (figure 6). The SWCNH–GNP–SWCNH conductive network and SWCNH–SWCNH conductive paths at the outer surface of the bead create difficulty for the microwave to escape from sample before absorption. Thus, we got an enhanced SE_A with the increase of bead loading in the nanocomposites (figure 7b). The maximum microwave absorption (~85.6 %) was achieved for SWCNH/GNP/PMMA nanocomposites at 1.072 vol% SWCNH and 70 vol% GNP/PMMA bead loading. The SE_R value also increases with the increase of SWCNH and GNP/PMMA bead loadings in the nanocomposites.

The impedance mismatch between air and materials increases with the increase of filler (SWCNH and GNP) loading. Thus, reflection shielding (14.16%) was achieved for the 1.072 vol% SWCNH and 70 vol% GNP/PMMA bead containing SWCNH/GNP/PMMA

nanocomposites. It is assumed that the SWCNH-GNP-SWCNH conductive network also facilitates the microwave reflection in the nanocomposites.

Complex permittivity and permeability analysis

For further investigation of the EMI Shielding characteristic, the Nicholson-Ross-Weir[20] method was followed to evaluate the complex permittivity (ε^*) of the SWCNH/GNP/PMMA nanocomposites from the S parameter. The complex permittivity consists of real (ε') and imaginary (ε'') part.

$$\varepsilon^* = \varepsilon' + i_0\varepsilon'' \qquad (14)$$

The polarization loss is the real part and the electric loss is the imaginary part of complex permittivity. Figure 8 displays that the frequency dependent complex permittivity (real and imaginary) of the SWCNH/GNP/PMMA nanocomposites varies on varying the loading of SWCNH and GNP/PMMA bead. The permittivity (real) of the nanocomposites increases with the increase of SWCNH and GNP/PMMA bead loading [Figure 8 (a) and (b)]. The numbers of micro capacitor and polarization centers are responsible for the real permittivity of the nanocomposites. The polarization center creates form the defects of the nanofiller structure.[32] The charge density between polymer matrix and nanofiller aggregation leads to the formation of micro capacitor in the nanocomposites. It can be assumed that many dead arms of SWCNH appears as micro capacitors and many number of polarization center in the nanocomposites due to its flower like structure and tendency of aggregation. Thus, with the increase of SWCNH loading the polarization center and micro capacitor increases which leads to enhance the real permittivity.

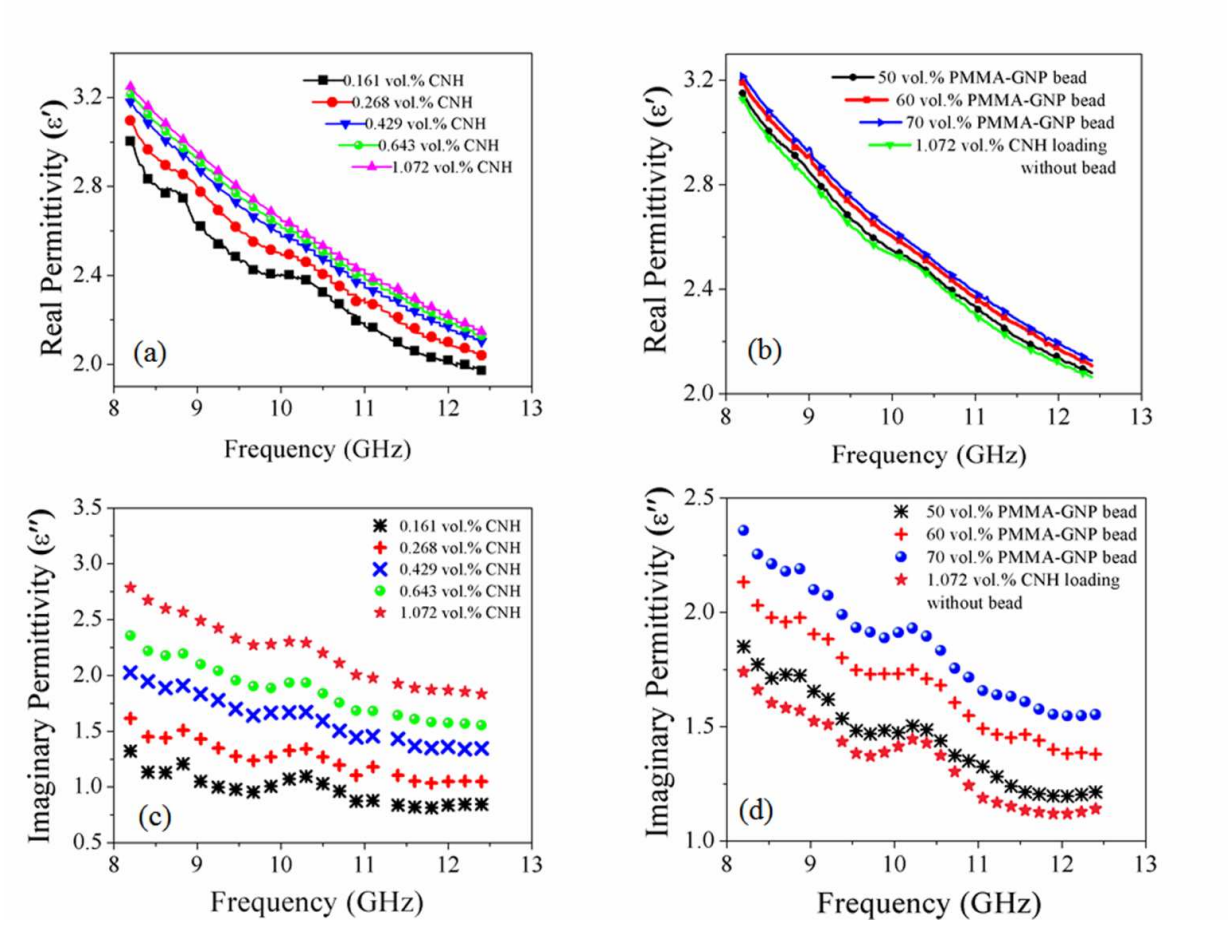

Figure 8: Real permittivity versus frequency at (a) different SWCNH loading with constant (70 vol%) GNP/PMMA bead loading, (b) different loading of GNP/PMMA bead with constant (0.643 vol%) SWCNH loading and imaginary permittivity versus frequency at (c) different loading of SWCNH containing constant (70 vol%) GNP/PMMA bead, (d) different GNP/PMMA bead loading with constant SWCNH loading (0.643 vol%) of the SWCNH/GNP/PMMA nanocomposites.

Furthermore, the non-conducting nature of the GNP/PMMA beads creates the impedance mismatch in the nanocomposites and the presence of GNP creates micro capacitor and polarization center in the nanocomposites. Thus, with the increase of GNP/PMMA bead loading at constant SWCNH loading, the real permittivity increases. Moreover, the gap between the

SWCNH decreases which increases the polarization of the polymeric materials with the increase of SWCNH loading and GNP/PMMA bead loading and consequently enhances the shielding efficiency by absorption. The number of conductive path and network increases with the increases of SWCNH and GNP/PMMA bead loading and through the conductive path and network the mobile charge dissipate. Thus, the imaginary permittivity, presenting the electric loss, increase with SWCNH and bead loading [Figure 8 (c) and (d)]. The higher imaginary permittivity leads to higher electromagnetic radiation dissipation in the nanocomposites (i.e. absorption).

The complex permeability (real and imaginary) of the SWCNH/GNP/PMMA nanocomposites was evaluated from the S parameter following the Nicholson-Ross-Weir method[20]. The real (μ′) and imaginary (μ″) part of complex permeability were decreased with increase in frequency (Figure 9). With the increase of SWCNH and GNP/PMMA bead loading the real part of the permeability decreases but the imaginary part of the permeability increases. The real parts and imaginary parts of complex permeability related with the energy storage and loss of electromagnetic wave in materials.[33] The positive imaginary permeability value indicate that the incident electromagnetic energy absorbed by the absorber and the negative imaginary permeability is consider as the electromagnetic energy going out from the absorber.[34] Thus, positive imaginary value indicates that the microwave absorption increases in the nanocomposites with the increase of SWCNH and GNP/PMMA bead loading.

Such a high permeability of the nanocomposites can be described in terms of the presence of SWCNH in the nanocomposite. SWCNH shows a unique magnetic property due to its structure. SWCNH consisting of ~10000 carbon atoms has at least one unpaired electron spin. It can be assumed that the unpaired electron spin originated from the electronic structure of the

nanohorn tips and thus, the expected large diamagnetism (developed from the presence of large number of double bond in SWCNH) is cancelled by Van Vleck constant Paramagnetism. Thus small diamagnetic susceptibility is observed for SWCNH.[35] Researchers also have found Curie-Weiss-paramagnetism,[35,14] antiferromagnetism[36] property for the SWCNH. Like SWCNH, even with CNT, Yun et al. reported high permeability for PVA/PAAC composite using MWCNT without any magnetic particle.[37]

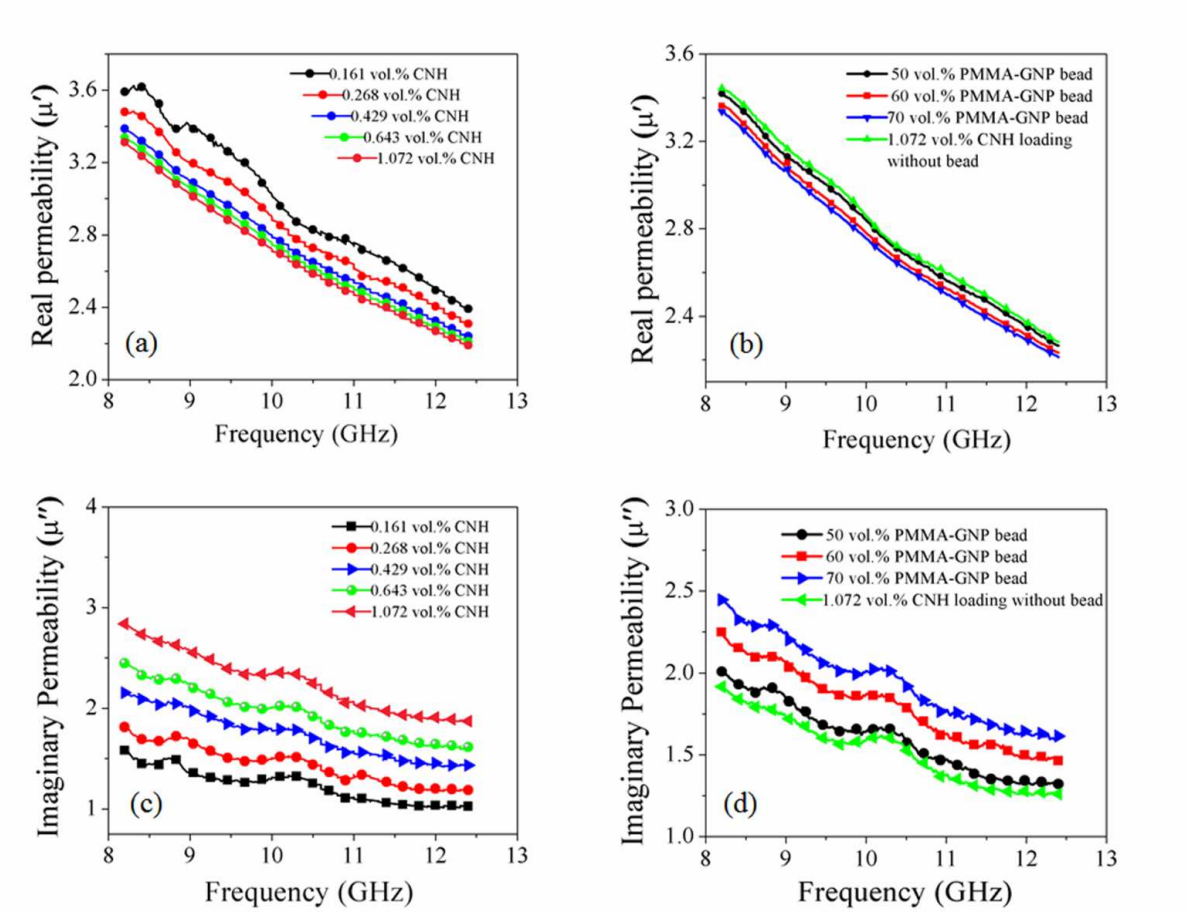

Figure 9: The variation of real permeability in X band frequency region with (a) different SWCNH loading at 70 vol% GNP/PMMA bead loading ,(b) different loading of GNP/PMMA bead containing (0.643 vol%) SWCNH and imaginary permeability with (c) different SWCNH

loading at 70 vol% GNP/PMMA bead, (d) different GNP/PMMA bead loading at constant SWCNH loading (0.643 vol%) of the nanocomposites.

Conclusion

SWCNH/GNP/PMMA nanocomposites were prepared through incorporation of suspension polymerized GNP/PMMA bead in the *in-situ* polymerized SWCNH/PMMA matrix during the polymerization reaction. A considerably high value ~ (–23.6 dB) of EMI SE and conductivity (4.54×10^{-2} $S.cm^{-1}$) were achieved in the nanocomposites with SWCNH:GNP:PMMA = 1.072 vol% (1.0 wt%) : 0.089 vol% (0.175 wt%) : 98.839 vol% (98.825 wt%). In the prepared nanocomposites the percolation threshold was also significantly reduced to 0.11 vol% of SWCNH. The architecture of nanocomposites was assumed to be responsible for such a high conductivity and EMI SE value. The unique architecture was achieved due to the presence of beads in the nanocomposites. The presence of bead acted as excluded volume which facilitated the formation of SWCNH-SWCNH conductive path and GNP-SWCNH-GNP or SWCNH-GNP-SWCNH network structure. The presence of bead attenuate the microwave energy through reflection and the nonconductive GNP/PMMA beads creates dielectric mismatch in the nanocomposites which influenced the reflection and internal multiple reflection property of materials. Moreover, the contribution from flower like geometry and electrical property of SWCNH in microwave absorption facilitate to achieve such a high EMI SE value. The AC conductivity and dielectric permittivity of the nanocomposites were increased with increase in SWCNH, as well as, bead loading, i.e., with increase in effective concentration of conductive nanofillers. The thermal stability and tensile property of the prepared nanocomposites also increases compared to the pure polymer.

Acknowledgements

We thank the University Grant Commission (UGC), India for their financial support.

References:

[1] J. M. Thomason, D. Vulug, M. Alexandre, C. Jerome, I. Molenberg, I. Huynen, C. Detrembleur, *Polymer,* 2012, **53**, 169-174.

[2] Z. Liu, G. Bai, Y. Huang, Y. Ma, F. Du, F. Li, T. Guo, Y. Chen, *Carbon,* 2007, **45**, 821-827.

[3] D. X. Yan, P. G. Ren, H. Pang, Q. Fu, M. B. Yang, Z. M. Li, *J. Mater. Chem.* 2012, **22**, 18772-18774.

[4] J. Joo, H. M. Kim, K. Kim, C. Y. Lee, S. J. Cho, H. S. Yoon, D. A. Pejakovic, J. W. Yoo, A. J. Epstein, *Appl. Phys. Lett.* 2004, **84**, 589−591.

[5] Y-L. Huang, S-M. Yuen, C-C. Ma, C-Y. Chuang, K-C. Yu, C-C. Teng, H-W. Tien, Y-C. Chiu, S-Y. Wu, S-H. Liao, F-B. Weng, *Comp. Sci. Tech.* 2009, **69**, 1991–1996.

[6] Y. Yang, M. C. Gupta, *Nano Lett.* 2005, **5***,* 2131-2134.

[7] Y. Huang, N. Li, Y. Ma, F. Du, F. Li, X. He, X. Lin, H. Gao, Y. Chen, *Carbon.* 2007, **45**, 1614-1621.

[8] M. C. Gupta, Y. Yang, K. L. Dudley, R. W. Lawrence, *Adv.Mater.*2005, **17**, 1999−2003.

[9] D. X. Yan, H. Pang, B. Li, R. Vajtai, L. Xu, P. G. Ren, J. H. Wang, Z. M. Li, *Adv. Funct. Mater.* 2015, **25**, 559-566.

[10] J. Ling, W. Zhai, W. Feng, B. Shen, J. Zhang, W. G. Zheng, *ACS Appl. Mater. Interfaces.* 2013, **5**, 2677-2684.

[11] Y. Fukunaga, M. Harada, S. Bandow, S. Iijima, *Appl. Phys. A.* 2009, **94**, 5

[12] K. Urita, S. Seki, S. Utsumi, D. Noguchi, H. Kanoh, H. Tanaka, Y. Hattori, Y. Ochiai, N. Aoki, M. Yudasaka, S. Iijima, K. Kaneko, *Nano Lett.* 2006**, 6**, 1325-1328.

[13] S. Zhu, G. Xu, *Nanoscale*. 2010, **2**, 2538–2549.

[14] S. Garaj, L. Thien-Nga, R. Gaal, L. Forro, K. Takahashi, F. Kokai, M. Yudasaka, S. Iijima,*Physic. Rev. B.* 2000, **62**, 17115-17119.

[15] S. Berber, Y. K. Kwon, D. Tomanek, *Phys. Rev. B.*2000, **62**, R2291-R2294.

[16] D. V. Kolesnikov, V. A. Osipov, *JETP Lett.* 2004; **79***,* 532-536.

[17] L. Ning, Y. Huang, D. Feng, H. Xiaobo, L. Xiao, G. Hongjun, M. Yanfeng, F. Li, Y.Chen, P. C. Eklund, *Nano Lett.* 2006, **6**, 1141-1145.

[18] J. M. Thomassin, C. Jerome, T. Pardoen, C. Bailly, I. Huynen, C. Detrembleur, *Mater. Sc. Eng. R.* 2013, **74**, 211–232.

[19] M. H. Al-Saleh, W. H. Saadeh, U. Sundararaj, Carbon. 2013, 146 – 156.

[20] A. M. Nicolson, G. F. Ross, *IEEE Transactions on Instrumentation and Measurement,* 1970, **19***,* 377-382..

[21] A. F. Szczypta, S. Blazewicz, *J. Mater. Sci.* 2011. **46***,* 5680-5689.

[22] S. Kirkpatrick, *Rev Mod Phys.* 1973, **45**, 574–88.

[23] D. Stauffer, A. Aharony, *2nd ed. London: Taylor and Francis*; **1992**.

[24] N. K. Shrivastava, P. Kar, S. Maiti, B. B. Khatua*. Polym Int.* 2012, **61,** 1683–1692.

[25] R. Fisch, A. B. Harris, *Phys. Rev. B.* 1978, **18**, 416-420.

[26] D. B. Gingold, C. J. Lobb, *Phys. Rev. B.* 1990, **42**, 8220–8224..

[27] M. A. Pantoja-Castro, J. F. Pérez-Robles, H. González-Rodríguez, Y. Vorobiev-Vasilievitch, H. V. Martínez-Tejada, C. Velasco-Santos. *Mater.Chem.Phys*. 2013,**140** 458-464.

[28] D. D. L. Chung, *J. Mater. Eng. Per.* 2000, **9**, 350-354.

[29] B. Yuan, L. Yu, L. Sheng, K. An, X. Zhao, *J Phys D Appl Phys.* 2012, **45**, 235108(1-6).

[30] A. Gupta, V. Choudhary, *Comp Sci. Tech,* 2011, **71**, 1563-1568.

[31] Y.-Y. Kim, J. Yun, H.-I. Kim, Y.-S. Lee, *J. Ind. Eng. Chem*. 2012, **18**, 392-398.

[32] P. C. P. Watts, W.-K. Hsu, A. Barnes, B. Chambers, *Adv. Mater,* 2003, **15**, 600-603.

[33] X. F. Zhang, H. Huang, X. L. Dong, *J. Phys. Chem. C*. 2013, **117**, 8563 −8569.

[34] J. C. Wang, X. Han, X. Zhang, S. Hu, T. Zhang, J. Wang, Y. Du, X. Wang, P. Xu, *J. Phys. Chem. C.* 2010, **114**, 14826–14830.

[35] S. Bandow, F. Kokai, K. Takahashi, M. Yudasaka, S. Iijima, *Appl. Phys. A,* 2001, **73**, 281–285.

[36] H. Imai, P. K. Babu, E. Oldfield, A. Wieckowski, D. Kasuya, T. Azami, Y. Shimakawa, M. Yudasaka, Y. Kubo, S. Iijima, *Phys. Rev. B,* 2006, **73**, 125405.

[37] J. Yun, J. S. Im, Y.-S. Lee, H.-Il Kim, *Eur. Poly. J.* 2010, **46,** 900–909.